Nuclear Materials and Energy 12 (2017) 1253–1258

Contents lists available at ScienceDirect

Nuclear Materials and Energy

journal homepage: www.elsevier.com/locate/nme

Thomson scattering of plasma turbulence on PSI-2

M. Hubeny[a,*], B. Schweer[a], D. Luggenhölscher[b], U. Czarnetzki[b], B. Unterberg[a]

[a] Forschungszentrum Jülich GmbH, Institut für Energie- und Klimaforschung Plasmaphysik, 42425 Jülich, Germany
[b] Institut für Plasma und Atomphysik, Ruhr-Universität Bochum, 44780 Bochum, Germany

ARTICLE INFO

Article history:
Received 15 July 2016
Revised 22 November 2016
Accepted 7 December 2016
Available online 27 December 2016

Keywords:
Fusion
Plasma diagnostic
Thomson scattering
Turbulence
Conditional average

ABSTRACT

The turbulent transport in the edge of fusion reactors can be conveniently simulated by linear plasma devices with long duty cycles. At high input power steady state plasma discharges at PSI-2 exhibit intermittent fluctuations similar to the edge of toroidal plasma devices. As their influence on erosion predictions is obscured by time-averaged measurements a time-resolved Thomson scattering setup is installed and tested at PSI-2. Aided by a fast CMOS camera and conditional averaging a time resolution of 3 µs was achieved for temperature and density profile evolution in Argon and Deuterium discharges. A 40 kHz, m = 1 oscillation with 50 µs coherence time and 1 eV electron temperature amplitude was identified in Argon, while in Deuterium intermittent events were associated with a 4 eV rise in edge temperature and a 10% reduction of bulk density.

1. Motivation

Linear plasma devices are widely used to study fundamental plasma characteristics and were able to simulate turbulent particle and heat transport representing first wall [1–3] or even divertor [4] conditions of fusion reactors. For the performance of fusion reactors turbulent transport has been an obstacle since the beginning of fusion research and the ever increasing understanding of plasma transport answers questions about confinement, but raises new ones regarding the influence of turbulence on erosion. Driven by strong pressure gradients in the edge of magnetically confined plasmas this turbulent transport can constitute a large fraction of the plasma transport [5,6] and manifests itself as filamentary intermittent events (synonym to blob/avaloid), being found in (virtually all) toroidal and linear plasma devices [7].

While the understanding of intermittent transport and its influence on plasma wall interaction is still incomplete experimental scalings towards steeper gradients (favorable for compact reactors) point to larger and radially faster filaments leading eventually to a convective transport regime comprised of these intermittent events [8]. Since the density shoulder flattens in these regimes the (faster) filaments could reach the first wall in a reactor. Plasma wall interaction processes which depend non-linearly on the plasma temperature, e.g. physical sputtering, are thus affected by the statistics of the fluctuating plasma temperature. A common statistical identification of the intermittency of fluctuations, skewness and kurtosis, is always found to be positive for density/temperature measurements in the plasma edge, which could lead to increased erosion by filaments [9] or hotter charge-exchange neutrals [10].

The application of laser Thomson scattering (TS) to low density plasmas has been demonstrated extensively [11] and the interpretation of incoherent TS is rather straightforward compared to other methods, although it requires more sophisticated instrumentation and integration over long times. While this usually eliminates the possibility of time-resolved measurements, regularly occurring plasma phenomena were resolved by triggering the laser according to e.g. an oscillation of the discharge voltage [12] to find oscillating plasma parameters. Recently, the modulation of the electron velocity distribution in an inductively coupled plasma was demonstrated by phase locking the laser trigger to the RF generator of the plasma [13]. However, these techniques are applicable for stable oscillations and/or long coherence times. Fast, intermittent and unpredictable dynamics require a technique which does not integrate the scattered Thomson signal, but retains the temporal information for later reconstruction. Furthermore, TS allows unique access to the energy distribution function and thus additional insight to explain captured plasma dynamics.

Fast framing CMOS cameras record the fast dynamics of the turbulence, but integrate plasma emissions over a wide spectral range. A combination of TS and a fast framing camera with convenient long measurement times in a steady state linear plasma device like

* Corresponding author.
E-mail address: m.hubeny@fz-juelich.de (M. Hubeny).

http://dx.doi.org/10.1016/j.nme.2016.12.006

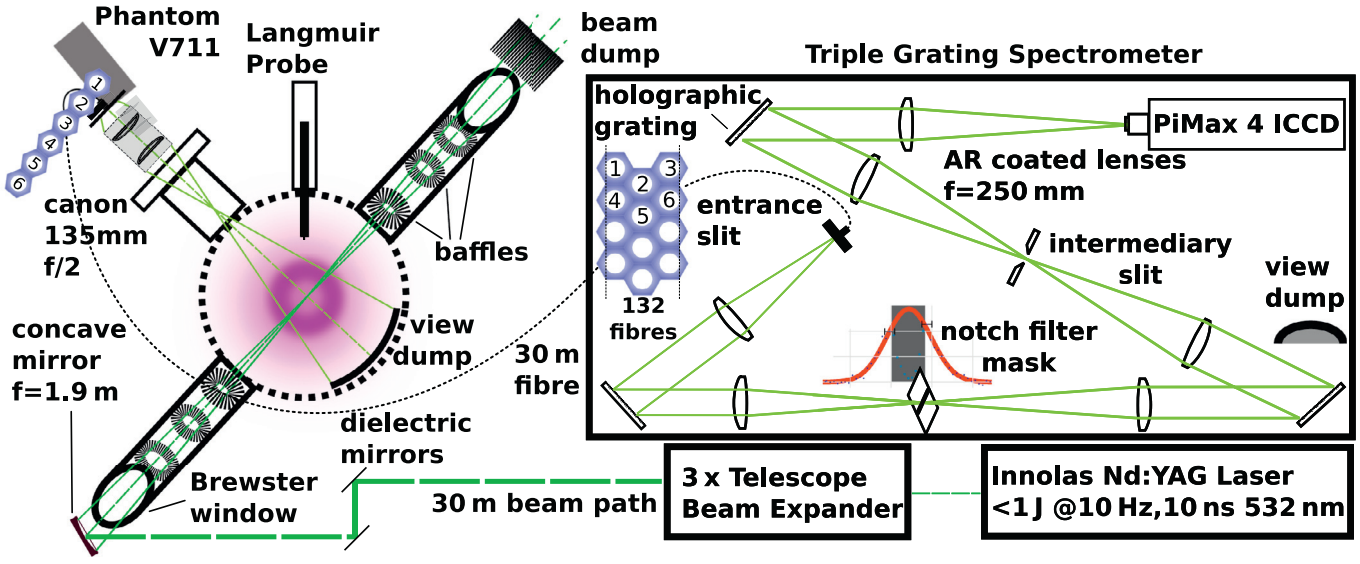

Fig. 1. Schematic view of all components of TS diagnostic including PSI-2 chamber.

PSI-2 enables measurements of average density and temperature with the fluctuation dynamics in the edge of the plasma by using a conditional averaging method. To preserve the temporal information in TS a photon counting method (similar to [14]) is used. Thus, the information of the fast dynamics in the CMOS camera are used as a later software trigger for combining TS signal fulfilling the averaging condition. The goal for the diagnostic method is to investigate intermittent events with the accuracy of TS in density and temperature, retaining a high temporal resolution.

2. Experimental setup and method

PSI-2 is a steady-state linear plasma generator, which was recently equipped with a Thomson scattering diagnostic setup. Working gases for the arc-discharge operated device include hydrogen, deuterium and various noble gases, which constitute a plasma of roughly 6–8 cm diameter in a magnetic field of ~100 mT. PSI-2 is used for studies on plasma wall interaction and a forerunner experiment to test diagnostics and sample handling for JULE-PSI, where activated samples will be exposed. Details on the operation and diagnostic setup of PSI-2 can be found in [15]. For this study high-power, low gas-feed discharges were used in Argon and Deuterium. The complete diagnostic TS setup is shown in Fig. 1 and starts with a Nd:YAG laser (Innolas Spitlight 2000) operated at the second harmonic wavelength of 532 nm, with a frequency of 10 Hz and a maximum pulse energy of 1,2 J. Since this energy exceeded the damage threshold of the aluminum coating on the focusing mirror the actual pulse energy had to be reduced to 400–700 mJ, measured at the beam dump. The laser beam is expanded three-fold in a Galilean type telescope and then guided to the PSI-2 plasma chamber over a distance of 30 m by six dielectric mirrors of which three are remotely motor controlled. Finally, the laser spot with 3 cm diameter is focused with a custom-made focusing mirror with a focal length of 1.9 m. Position control of the laser beam was realized via surveillance cameras observing the diffuse reflection of the laser beam with high exposure times (to avoid flickering) behind 1% gray filters. The coupling of the laser in and out of the vacuum chamber consists of two Brewster windows mounted on the end of long tubes containing baffles.

Triple grating spectrometer. The TGS is a fiber-coupled version of [14,16] and designed for high throughput and stray-light rejection. A radial profile of 13 cm is focused by a 135 mm F/2 Canon lens onto 132 fibers with a diameter of 250/275 µm (core/cladding). Each fiber collects light from a circle of about 1 mm diameter. The fibers are rearranged in pairs of three according to Fig. 1 and constitute the entrance slit of ~750 µm of the TGS. The physical notch filter in the TGS design provides a blocking ratio of the central laser wavelength surpassing any optical filter. The intermediary slit blocks stray-light from within the TGS to reproduce the original slit without the laser signal, but can also be used to reduce the effectively used slit and increase the spectral resolution, e.g. for calibration purposes. Finally, the PiMax 4 camera with a Gen3 sensor and fiber-coupled image intensifier records the scattered spectrum with a minimal shutter speed of 3 ns at twice the laser repetition rate and in photon counting mode, i.e. every trigger is read out immediately. In this way, the plasma background is measured simultaneously, dark current is negligible and the received photons are discriminated against the readout noise only.

Photon counting. To achieve a frame rate of 20 Hz 4 pixels on the CCD chip are binned in the radial direction and the common Matlab ™ *findpeaks* routine is applied vertically and horizontally along each frame and line. All the found peaks are added logically (AND operation) to avoid double-counting of a single photon signal spread over several pixels. Nevertheless, the summation of all surrounding pixel counts is necessary to account for two photon events. The threshold for two photons is a total of 1000 counts, while the average single photon event produces 350–400 counts. Using this average count rate per photon the photon counting method is in agreement with the usual CCD integration of signal.

Fast camera. The fast framing, monochrome CMOS camera Phantom V711 is used at a reduced resolution of 256/384 (radial) by 16 (axial) pixels to enable a frame rate of f_s = 330 kHz synchronous to TS. Higher frame rates (0.6-1 MHz) are used in stand-alone videos. A f = 18-35 mm, F/1.8 wide-angle lens was used at f = 24 mm to image a radial profile of 20 cm, while the axial pixels are software binned. The depth-of-field is approximately 6 cm and the focus is in the same plane as the TS laser but shifted about 1 cm axially to avoid direct laser stray-light, while its reflection in the chamber is used for synchronization. The brightness signal is imaged by the CMOS camera without filters, since there are multiple lines emitting in Argon. In deuterium D_α is the strongest line,

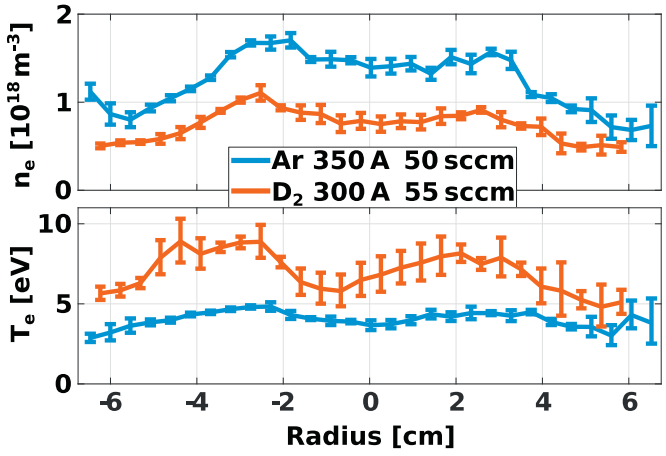

Fig. 2. TS equilibrium profiles of n_e and T_e in Argon and Deuterium.

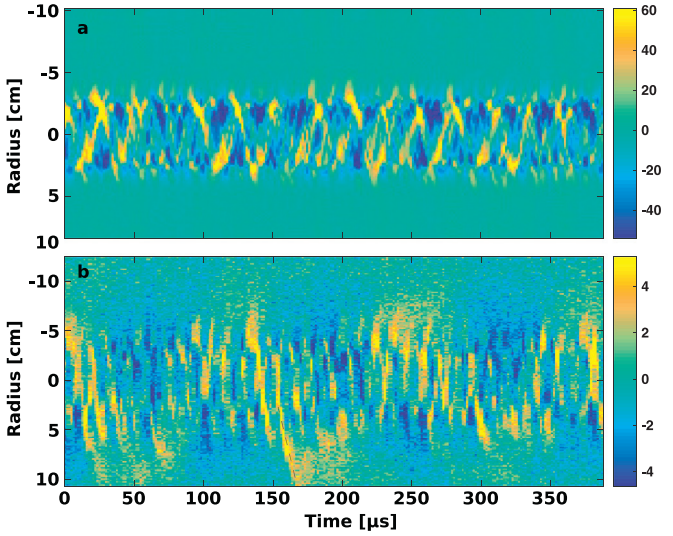

Fig. 3. Profile evolution of brightness fluctuations compared for Argon (a) and Deuterium (b) discharge.

but a filter transmits only 50% even at the design wavelength and thus reduces the maximum shutter speed.

Timing scheme. Since the laser and TGS are only 5 m apart and laser path and optical fibers each 30 m in length, there is no need for a dedicated timing generator, but the Pockels cell (PC) trigger output is used directly to trigger the PiMax camera. The PC trigger is guided to a LeCroy crate and repeated after 50 ms to create a 20 Hz trigger. The jitter of 1 ns observed by an oscilloscope is acceptable and accounted by setting the shutter time to 10 ns, while the stated laser waveform has a 7 ns length. Scanning with the minimal shutter speed of 3 ns across the laser waveform confirmed the usage of a 10 ns gate length. In order to observe the plasma state by the fast camera before the laser shot, the flashlamp trigger (FL) is used for the fast camera similar to the PC trigger. The rising edge of the FL trigger is guided to the LeCroy crate, doubled and send by BNC to the fast camera. For its $1/f_s = 3$ μs accuracy a jitter between FL and PC trigger is not observable and the fast camera is triggered sufficiently accurate about 200 μs before the laser beam arrives in the chamber. The camera is used in burst mode such that every FL trigger causes the recording of only 100 frames at f_s, reducing overall memory consumption and easing analysis and synchronization. The frame in which the laser reflection is visible is delayed to frame 55 to access the plasma state about 140 μs before and after the TS measurement.

3. Results

Fig. 2 shows equilibrium profiles obtained by TS for discharges in Argon (a) and Deuterium (b) based on 21,000 and 42,000 laser shots at an average energy of 660 mJ and 620 mJ per pulse, respectively. The profiles of n_e and T_e are compared. The absolute calibration of n_e was performed by Raman scattering on Nitrogen before and after the discharges at pressures in the range of 10–30 mbar in the PSI-2 chamber, following the procedure described in [16,17]. The pressure is converted to the number density of scattering centers in Nitrogen by using the chamber temperature, while the total cross-sections of RS and TS are known. Then the total scattered power ratio between RS and TS corresponds directly to the ratio of electron density to nitrogen gas density, eliminating the influence of the collecting solid angle, optical efficiencies and laser power, provided these quantities are constant or accounted for drift/deliberate change. The spectral calibration was done with a Neon discharge lamp at an intermediate slit width of 100 μm. The fibers are back-illuminated and focused on a scale metal plate at the laser plane for spatial calibration. The discharges are carried out with high currents of 350 A/300 A and low gas feeds of 50/55 sccm, resulting in a power coupling to the plasma of 25–30 kW. Both profiles show a slightly hollow n_e and T_e profile with a maximum at r = ± 2–3 cm. The density in Argon reaches 1.8 × 10^{18} m^{-3} and 1.6 × 10^{18} m^{-3} in the peaks and drops of after r = ± 3 cm, while the n_e profile peaks at the same radial position but at 1 × 10^{18}m^{-3} in Deuterium. In contrast, the temperature reached in Argon is much lower than Deuterium (4.5 eV–9 eV).

Qualitatively, these findings agree with Langmuir probe measurements insofar the profile shape of plasma temperature and density are concerned. Higher temperatures and lower densities for like powered Deuterium discharges compared to Argon are confirmed, while the absolute figures differ by a factor of roughly 2. One of the most critical issues is probably the anisotropy caused by the magnetic field which make Langmuir probe measurements difficult to interpret quantitatively, especially for absolute density determination since the effective collecting area is not well defined. Furthermore, the probe is situated about 10 cm axially upstream and measures only one side of the profile vertically, whereas the TS profiles are inclined 55° from the vertical axis. However, this may only account for part of the deviation, since azimuthal and short axial variations of plasma parameters are small.

The error for TS results is estimated by the combination of standard deviation of the signal time series in each pixel channel and the confidence level of the fit routine for the spectra. The plasma background is subtracted immediately and before and after each discharge the laser stray light is measured and subtracted as well. The systematic error for the Raman calibration is dominated by the 8% uncertainty of the anisotropy polarizability for calculating the Raman scattering cross-section in [18].

3.1. Dynamics

Fig. 3 compares a sample of the brightness profile evolution of the plasma column for a discharge with Argon (a) and Deuterium (b), respectively. The mean profile is subtracted and only the fluctuating parts are shown. The Argon profiles show a clearly visible, periodic oscillation in its brightness. The oscillation is not coherent in time and also the mode number is not stable, while the m = 1 mode is the most prominent. A Fourier analysis shows a single frequency (f = 40 kHz) with its harmonics. In contrast, the Deuterium discharge shows large outreaching structures. While the oscillation in the main plasma is in the order of 80 kHz, there is an additional faint slow oscillation (∼10 kHz) which is only

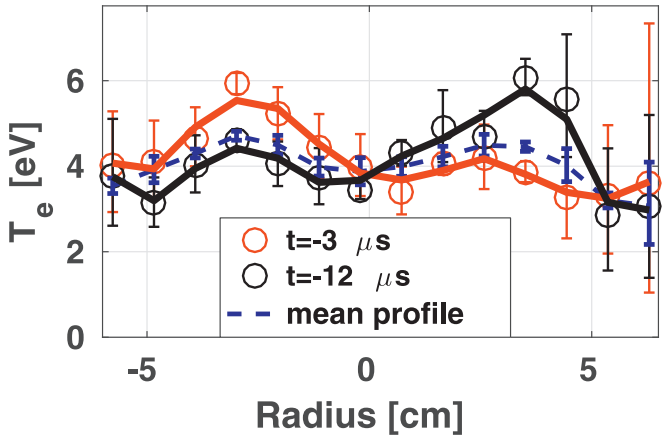

Fig. 4. T_e profiles for CA case t = −12 μs (black) and t = −3 μs (red) compared to the average T_e profile (blue). (For interpretation of the references to color in this figure legend, the reader is referred to the web version of this article.)

present in the plasma edge. A typical example of a strong intermittent event is shown in Fig. 3b at positive radii beginning at t = 160 μs, indicated by the dashed line. The radially projected velocity estimated by the slope of the line is ∼5.6 km/s, while an underlying azimuthal movement would require higher velocities, which are in the range of the phase velocities of the oscillations (10–15 km/s).

The low gas-feed discharges have been selected for investigation for the ion-neutral collisions stabilize instabilities by friction and thus using a low gas flow rate allows a more turbulent plasma. However, the higher ion mass of Argon also has a stabilizing effect due to the inertia of ions slowing down the dynamics of the electrons. This explains the qualitative difference between the two discharges, while the exact type of instability is uncertain due to missing spatial information. A resistive drift wave model was successfully employed to explain intermittent dynamics at NAGDIS-II in [19] and simulations are ongoing for PSI-2.

Since the Argon discharge produces a tenfold higher brightness signal with slower dynamics and its higher TS signal due to the higher equilibrium density, the Argon discharge is now presented as a test case for the diagnostic method and then the Deuterium discharge is analyzed focusing on the intermittent events at the plasma edge.

Time-resolved TS on Argon discharge. About 14,000 out of 21,000 shots were recorded synchronously with each 100 frames of the fast camera and can be used for the time-resolved analysis. For these shots the conditional averaging is triggered, i.e. the shot is part of the TS analysis, at a certain radial position in the fast camera data and above a fluctuation level threshold expressed in standard deviations σ. The trigger time of the CA can theoretically be set from frame 1 to 100, but for a proper recognition of the plasma state it is limited hereafter to 35 frames before and after the laser containing frame. The conditional averaging creates a decaying oscillation with its maximum at the trigger time, but the TS measurements are always obtained at frame 55. Thus, by cycling through all the time shifts the average structure is measured with the time resolution of the fast camera. Fig. 4 shows examples of T_e profiles corresponding to the plasma state at t = −3 μs and t = −12 μs (respective to CA trigger time) compared to the equilibrium profile. As the subset contains only about 1600 laser shots the statistical errors are increasing, yet the deviation of the two opposite phases of the oscillation are beyond the error at the profile maxima. To increase the accuracy for the subsets the radial resolution was reduced by a factor of two. The complete analysis over 71 frames in 3 μs time steps, centered around the laser shot containing frame, is shown in Fig. 5. First, Fig. 5a shows the 71 brightness profiles shifted by each trigger time and added to compose the average evolution of the oscillation in time. The T_e profile is shown in Fig. 5b for the subset data corresponding to shifting the CA trigger time continuously from t = − 105 μs to t = + 105 μs.

Fig. 6 cuts across the previous 2D evolution and shows the average of 3 time traces centered around r = ± 2.3 cm without their mean values together with the so far neglected TS n_e evolution. The resemblance of the brightness signal is clearly visible in the T_e profile evolution in Fig. 5 as well as in the traces in Fig. 6. The oscillation in T_e and brightness is matching in phase and in the decay of its amplitude. While the brightness images the complete, seeming rotation, visible in the center of Fig. 5a, the TS profiles lack the connection between the maxima. This is caused by the fast camera depth-of-field of 6 cm, which images the rotation also out of the laser plane, while the TS signal is strictly emitted and collected from the laser beam diameter. The amplitude of the T_e oscillation is about 1 eV corresponding to 20% of the T_e = 4.5 eV average value at the profile maxima. The frequency of this oscillation is f = 40 kHz, which is consistent with the brightness power spectrum, obtained without conditional averaging. The correlation

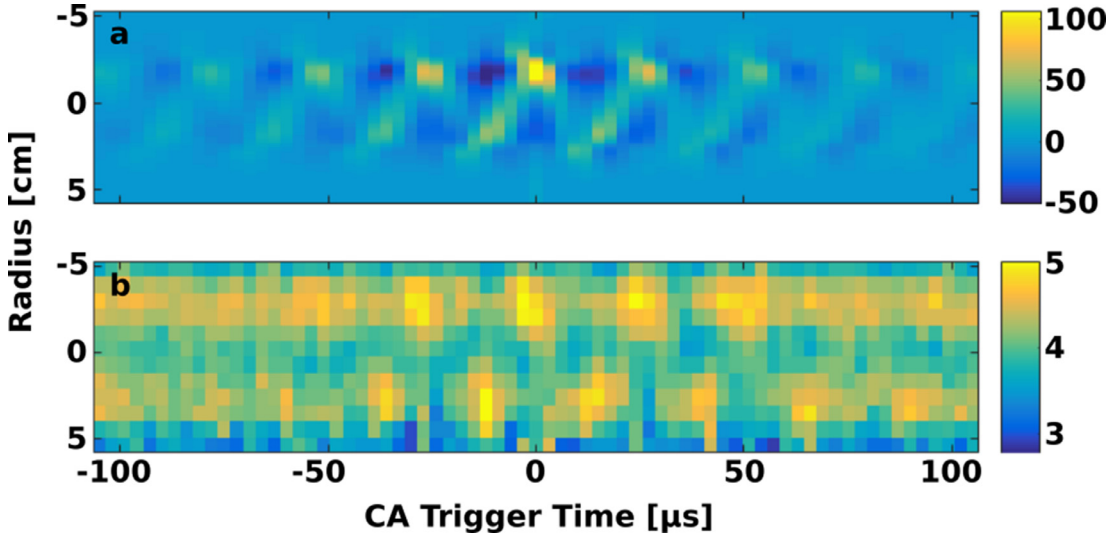

Fig. 5. CA of brightness and T_e in eV for Argon.

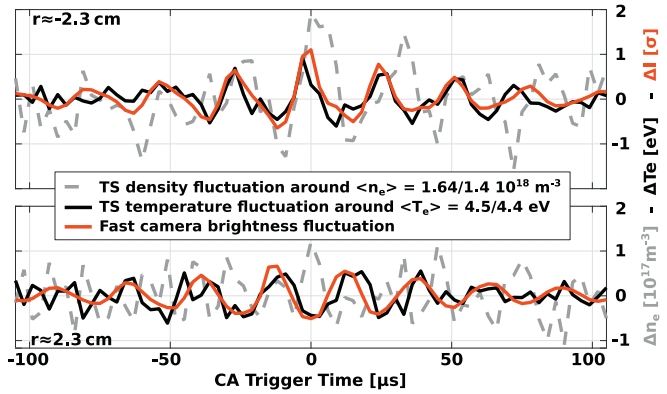

Fig. 6. Traces of n_e, T_e and brightness in upper and lower maxima.

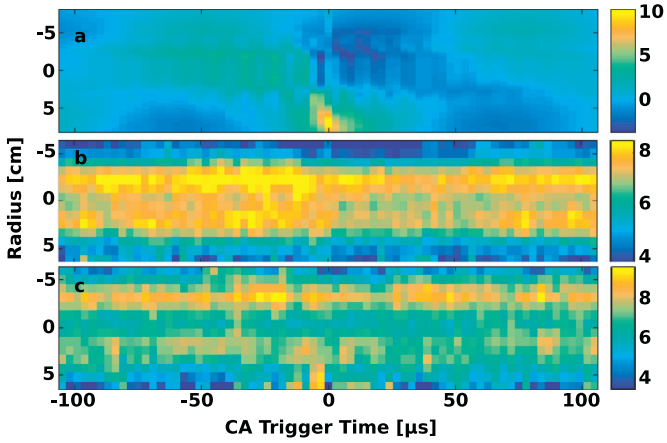

Fig. 7. CA of brightness, n_e and T_e in Deuterium.

time of the oscillation is estimated to $t_\tau \approx 50\mu s$ by a fitted exponentially decaying envelope function.

The TS n_e misses resemblance in the brightness, although a significant increase of n_e by about $2 \times 10^{17} m^{-3}$ at t = 0-3 µs is visible at r = −2.3 cm and about half at r = 2.3 cm. If a stable phase and/or frequency relation is missing between T_e and n_e, oscillations of n_e average out in the process of the CA subset creation and only the initial maximum is retained.

Time-resolved TS on Deuterium discharge. For the time resolved analysis of the deuterium discharge a total of 42,000 laser shots were used. The creation of the subsets is done in the same way as for the Argon discharge, but the CA trigger is set at r = 7.24 cm with a threshold of $\sigma = 1.5$. The average subset contains about 3000 laser shots, thus the radial resolution was also reduced by a factor of two compared to the equilibrium profile analysis. Fig. 7a shows the CA of the plasma brightness. Since the frame rate is 330 kHz as compared to the 715 kHz in Fig. 3b, the intermittent event is imaged less sharp. A slow variation of the edge plasma is visible in the brightness as well as the increase of the core brightness and sudden darkening upon appearance or ejection of the intermittent event.

The n_e profile in Fig. 7b shows an increase of the bulk density and sudden decrease, but the fast oscillations from Fig. 3b are neither visible in the brightness nor in the density or temperature profile. However, the temperature profile evolution in Fig. 7c shows a sharp rise in the edge temperature. These dynamics are portrayed more detailed in Fig. 8. The time traces of the averaged density within r = ± 3 cm is compared to the average brightness in the same range and the edge temperature is compared to the

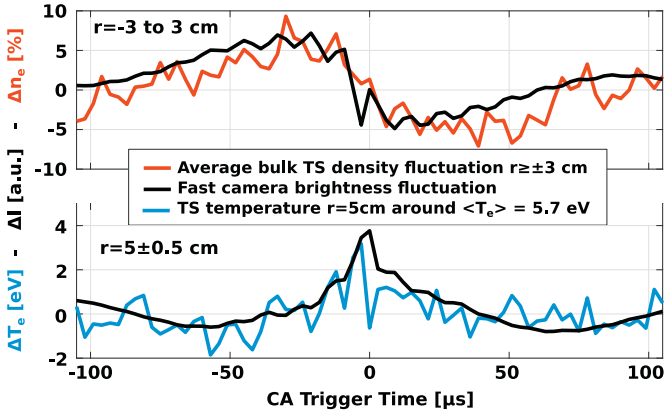

Fig. 8. Time traces of bulk n_e vs. bulk brightness and edge T_e vs. edge brightness.

edge brightness. Both brightness signals are adjusted in amplitude and fit remarkably well, despite comparing it to density and temperature. The bulk density drop around the intermittent event by about 10% or $7.5 \times 10^{17} m^{-3}$ could be explained by the expulsion of plasma. From the CA it is not clear whether there is an m = 0 mode responsible, since the 100 frames are not capturing the whole dynamics, yet the frame rate is too slow to resolve details. However, conclusions could be drawn from the free-running CMOS camera measurements with higher frame rates, where m = 1 and m = 2 modes grow rapidly and cause far reaching events shortly after. Furthermore, the onset and expulsion seems to be connected to a slower 10 kHz oscillation in the edge, since it is appearing in the CA. The transfer of free energy from lower to higher mode numbers is a likely explanation for intermittence, with the slow, outer oscillation pushing the growth rate of the emerging inner modes. The temperature rises significantly at the peak of the intermittent event and corresponds to the temperature in the maximum of the discharge. Since the time trace of the brightness exhibits a positive skewness of S = 0.5–1 in the edge, the temperature fluctuations likely posses the same statistical properties.

4. Conclusion

The proof-of-principle of using CA on TS has been demonstrated in Argon discharges, where the brightness is correlated to a 20% temperature fluctuation. In Deuterium intermittent events are partially resolved and likely responsible for the 10% bulk density drop. The intermittent event is linked to a significant temperature rise upon ejection.

Since the fluctuating pattern extracted by conditional averaging is consistent with free-running fast camera measurements, these and potentially faster dynamics are present in the plasma and the statistical properties of the brightness fluctuations apply to temperature fluctuations as well. This emphasizes the importance of including these fluctuations in processes concerning plasma wall interactions.

Both the TS system and the fast camera have potential for further improvements. The laser power restriction will be lifted with a dielectric mirror and an f = 2 m lens. The beam spot was about 2–3 mm during the present experiments, while 1 mm is the theoretically expected diameter, based on the laser divergence. The fast camera will be equipped with an F/1.4, 24 mm wide-angle lens, which will allow higher shutter speeds or the use of filters. Finally, the steady state character of the device allows for prolonged measurement times. With the increased signal the electron velocity distribution function becomes accessible for equilibrium measurements and the dynamic measurement gains certainty or time resolution.

Acknowledgments

This work has been carried out within the framework of the EUROfusion Consortium and has received funding from the Euratom research and training program 2014–2018 under grant agreement No 633053. The views and opinions expressed herein do not necessarily reflect those of the European Commission.

References

[1] T. Windisch, O. Grulke, T. Klinger, Phys. Plasmas 13 (12) (2006) 7, doi:10.1063/1.2400845. Article id. 122303.
[2] D.C. Pace, M. Shi, J.E. Maggs, G.J. Morales, T.A. Carter, Phys. Plasmas 15 (12) (2008) 13, doi:10.1063/1.3023155. Article id. 122304.
[3] S.H. Müller, C. Theiler, A. Fasoli, I. Furno, B. Labit, G.R. Tynan, M. Xu, Z. Yan, J.H. Yu, Plasma Phys. Control. Fusion 51 (5) (2009) 15, doi:10.1088/0741-3335/51/5/055020. Article id. 055020.
[4] N. Ohno, K. Furuta, S. Takamura, J. Plasma Fusion Res. 80 (4) (2004) 275–276, doi:10.1585/jspf.80.275.
[5] H.W. Müller, M. Bernert, D. Carralero, A. Kallenbach, B. Kurzan, A. Scarabosio, B. Sieglin, L. Tophøj, N. Vianello, E. Wolfrum, J. Nucl. Mater. 463 (2015) 739–743, doi:10.1016/j.jnucmat.2015.01.012.
[6] D. Carralero, H.W. Müller, M. Groth, M. Komm, J. Adamek, G. Birkenmeier, M. Brix, F. Janky, P. Hacek, S. Marsen, F. Reimold, C. Silva, U. Stroth, M. Wischmeier, E. Wolfrum, J. Nucl. Mater. 463 (2015) 123–127, doi:10.1016/j.jnucmat.2014.10.019.
[7] D.A. D'Ippolito, J.R. Myra, S.J. Zweben, Phys. Plasmas 18 (6) (2011) 48, doi:10.1063/1.3594609. Article id. 060501.
[8] D. Carralero, P. Manz, L. Aho-Mantila, G. Birkenmeier, M. Brix, M. Groth, H.W. Müller, U. Stroth, N. Vianello, E. Wolfrum, Phys. Rev. Lett. 115 (21) (2015) 215002, doi:10.1103/PhysRevLett.115.215002.
[9] G. Birkenmeier, P. Manz, D. Carralero, F.M. Laggner, G. Fuchert, K. Krieger, H. Maier, F. Reimold, K. Schmid, R. Dux, T. Pütterich, M. Willensdorfer, E. Wolfrum, T.A.U. Team, Nucl. Fusion 55 (3) (2015), doi:10.1088/0029-5515/55/3/033018. Article id. 033018.
[10] A. Mekkaoui, V. Kotov, D. Reiter, P. Boerner, Contrib. Plasma Phys. 54 (4–6) (2014) 409–414, doi:10.1002/ctpp.201410021.
[11] K. Muraoka, A. Kono, J. Phys. D 44 (4) (2011) 15, doi:10.1088/0022-3727/44/4/043001. Article id. 043001.
[12] W. Biel, A. Abou-El Magd, H. Kempkens, J. Uhlenbusch, Plasma Phys. Control. Fusion 37 (6) (1995) 599–610, doi:10.1088/0741-3335/37/6/001.
[13] D.L. Crintea, D. Luggenhölscher, V.A. Kadetov, C. Isenberg, U. Czarnetzki, J. Phys. D 41 (8) (2008) 6, doi:10.1088/0022-3727/41/8/082003. Article id. 082003.
[14] A. Kono, K. Nakatani, Rev. Sci. Instrum. 71 (7) (2000) 2716–2721, doi:10.1063/1.1150680.
[15] A. Kreter, C. Brandt, A. Huber, S. Kraus, S. Möller, M. Reinhardt, B. Schweer, G. Sergienko, B. Unterberg, Fusion Sci. Technol. 68 (1) (2015) 8–14. http://dx.doi.org/10.13182/FST14-906.
[16] M. van de Sande, Laser Scattering on Low Temperature Plasmas, Technische Universiteit Eindhoven, 2002 Ph.D. Thesis.
[17] E. Carbone, S. Nijdam, Plasma Phys. Control. Fusion 57 (1) (2015), doi:10.1088/0741-3335/57/1/014026. Article id. 014026.
[18] C. Penney, R. STPeters, M. Lapp, J. Opt. Soc. Am. 64 (5) (1974) 712–716, doi:10.1364/JOSA.64.000712.
[19] D. Reiser, N. Ohno, H. Tanaka, L. Vela, Phys. Plasmas 21 (3) (2014), doi:10.1063/1.4867492. Article id.032302.